Global Change Biology

WILEY

Global Change Biology

RESEARCH ARTICLE

Much Larger Whole-Profile Soil Organic Carbon Stocks on the Qinghai-Tibet Plateau Than Previously Reported

Jiajun Mao[1,2,3] | Shuai Zhang[1,2,3] | Mingming Wang[1,2,3] | Wu Yu[1,4] | Feng Liu[5] | Yuanhe Yang[6] | Mishra Umakant[7] | Zhou Shi[1,2,3] | Zhongkui Luo[1,2,3]

[1]State Key Laboratory of Soil Pollution Control and Safety, College of Environmental and Resource Sciences, Zhejiang University, Hangzhou, China | [2]Key Laboratory of Environment Remediation and Ecological Health, Ministry of Education, Zhejiang University, Hangzhou, China | [3]Zhejiang Key Laboratory of Agricultural Remote Sensing and Information Technology, Zhejiang University, Hangzhou, China | [4]College of Resources and Environment, Tibet Agricultural and Animal Husbandry University, Nyingchi, Tibet, China | [5]State Key Laboratory of Soil and Sustainable Agriculture, Institute of Soil Science, Chinese Academy of Sciences, Nanjing, China | [6]State Key Laboratory of Vegetation and Environmental Change, Institute of Botany, Chinese Academy of Sciences, Beijing, China | [7]Computational Biology and Biophysics, Sandia National Laboratories, Livermore, California, USA

Correspondence: Zhongkui Luo (luozk@zju.edu.cn)

Received: 10 September 2025 | **Revised:** 2 February 2026 | **Accepted:** 13 February 2026

Keywords: climate change | deep soil | mapping | permafrost | Qinghai-Tibet Plateau | soil organic carbon | spatial pattern

ABSTRACT

The Qinghai-Tibet Plateau (QTP), often referred as Earth's "Third Pole," is warming nearly twice the global average, potentially amplifying carbon–climate feedbacks to a greater extent than in most other regions. However, substantial uncertainties remain regarding the magnitude, spatial distribution, and environmental controls of the region's soil organic carbon (SOC) stocks. Here we compiled a comprehensive dataset of 2442 soil profiles across the QTP and integrated it with high-resolution (90 m) environmental covariates to generate spatially explicit, depth-resolved SOC stock estimates using machine learning models. Independent validation using newly collected whole-profile SOC measurements ($n = 53$) demonstrated substantially improved predictive accuracy compared to existing global and regional mapping products (e.g., SoilGrids, HWSD, and WISE). Specifically, our estimates reached coefficients of determination (R^2) of 0.63 and 0.49 for the 0–0.3 m topsoil and 0.3–1.0 m subsoil, respectively; while the existing mapping products only reached a R^2 of 0.01–0.35 in the topsoil and 0.01–0.15 in the subsoil. Across the QTP, our results estimated a total SOC stock of 62.0 (95% confidence interval: 54.9–69.1) Pg C within the top 2 m of soil, with more than 60% stored below 0.3 m depth. This value is much larger than most of the existing estimates in the same region. Alpine meadows ecosystems accounted for approximately 38% of the total SOC stock, primarily due to their extensive coverage, while swamp meadow ecosystems exhibited the highest SOC densities. Spatial uncertainty was highest in the sparsely sampled northwestern QTP. Contemporary climate and paleoclimate factors collectively contributed over 50% to the explained variance in SOC distribution across the soil profile, highlighting the dominant role of climatic factors on SOC spatial pattern. This spatially explicit, high-resolution SOC mapping provides a baseline for constraining carbon–climate feedback assessments on the QTP and underscores the region's heightened vulnerability to ongoing climate warming.

1 | Introduction

As an integral component of the terrestrial carbon cycle, soil organic carbon (SOC) plays a vital role in maintaining ecosystem productivity, regulating climate systems, and ensuring global food security (Schlesinger and Andrews 2000; Stockmann et al. 2015; Crowther et al. 2016). The spatial distribution and stability of SOC are governed by complex interactions among climatic, biotic, topographic, edaphic, and anthropogenic factors (Jenny 1941; Stockmann et al. 2015). Global environmental

change, particularly warming, threatens the stability of SOC pools globally (Schlesinger and Andrews 2000; Davidson and Janssens 2006; Zhang et al. 2024), posing substantial risks to long-term ecosystem function and carbon-climate feedback processes. This risk is particularly pronounced in cold regions where, on the one hand, they store a vast amount of SOC. For example, permafrost-affected high-latitude and high-altitude regions have SOC amounts of about 1300–1700 Pg C (Tarnocai et al. 2009; Hugelius et al. 2014; Schuur et al. 2015), accounting for more than half of the total SOC amount in global terrestrial soils. On the other hand, SOC in cold regions is more sensitive to global warming as low temperature has acted as a dominant rate-limiting control on SOC turnover (von Lützow and Kögel-Knabner 2009; Garcia-Palacios et al. 2024). An advanced understanding of SOC storage and dynamics in cold regions is vital for cold ecosystem management and for reliable prediction of global carbon cycle-climate feedbacks.

The Qinghai-Tibet Plateau (QTP), which is widely recognized as Earth's "Third Pole" (Mao et al. 2022), represents a such cold region and the world's largest high-altitude alpine system. Alpine soils often accumulate carbon over long timescales due to low temperatures and constrained decomposition. The plateau's grasslands, steppe meadows, and permafrost soils store substantial amounts of SOC and nutrients, and has been expected as a major component of the global SOC reservoir (Yang et al. 2008; Ding et al. 2016; Liang et al. 2019; Mu et al. 2020; Chen et al. 2024). Additionally, the QTP exerts a disproportionate influence on regional and global climate systems (Yang et al. 2020; Huang et al. 2023). The plateau is also a major cryospheric reservoir, hosting extensive glaciers, seasonal snow cover, and permafrost (Bolch et al. 2012; Zou et al. 2017; Yang et al. 2019; Kuttippurath et al. 2024). These components regulate surface energy balance, albedo, and hydrological timing. Together with grazing intensification and land use change, ongoing warming on the QTP—occurring two times faster than the global average (Slomp et al. 2013; Mu et al. 2020)—has cascading implications for carbon–climate feedbacks, including permafrost thaw, altered SOC stability, and changes in ecosystem services (Zhu et al. 2019; Wang et al. 2020; Wang, Lv, et al. 2022; Fu et al. 2025; Ren et al. 2025). Understanding SOC dynamics in this region is crucial for projecting carbon balances and for developing targeted management strategies for unique ecosystem services provisioned by the QTP and the relevant cold systems.

However, estimates of SOC stocks on the QTP focus on the 0–0.3 m topsoil with large uncertainties (Yang et al. 2009; Chang et al. 2014). Rare studies have extended to the whole soil profile at the regional scale (Ding et al. 2016, 2017; Wang 2022). Regional estimates of SOC stocks (SOC_s) across the QTP have been mainly conducted as part of either regional or global-scale mapping initiatives (Cao et al. 2013; Jiang et al. 2019; Wang et al. 2020; Mishra et al. 2021). However, substantial uncertainty persists in both the magnitude and spatial distribution of whole-profile SOC stocks, with estimates ranging from 30 Pg C to 40 Pg C (Yang et al. 2008; Mu et al. 2015; Zhao et al. 2018; Han et al. 2022; Wang 2022). These uncertainties primarily arise from two interconnected reasons. First, the QTP's complex climatic gradients, heterogeneous vegetation patterns, steep terrain, and extensive periglacial processes generate pronounced spatial and vertical heterogeneity in SOC stock, which is poorly captured by coarser-scale global products (Chen, Zhang, et al. 2022). In particular, geomorphic processes such as erosion, landslides, cryoturbation, and lateral redistribution of surface SOC further challenge traditional modeling approaches that rely solely on climatic and edaphic predictors (Chen, Zhang, et al. 2022). Second, past studies have employed diverse methodological approaches (e.g., geostatistical interpolation and diverse machine learning models) and datasets of varying quality and coverage (Ding et al. 2016, 2017; Zhao et al. 2018; Mishra et al. 2021; Han et al. 2022), further amplifying inconsistencies in SOC estimates. Consequently, accurately quantifying SOC stocks and elucidating their dominant environmental controls remain critical knowledge gaps for the QTP region.

We address the gap by developing a unified, large data-driven, and spatially explicit modeling framework for whole-profile SOC stock estimation at the resolution of 90 m with explicit evaluation of environmental drivers and uncertainties. We first compiled a comprehensive dataset of 2442 soil profiles with measured SOC, coupled with high-resolution environmental covariates including climatic, edaphic, topographic, vegetative, and anthropogenic variables. Using this comprehensive dataset, we trained a machine learning model—random forest (RF)—to predict SOC_s across three depth layers (0–0.3, 0.3–1.0, and 1.0–2.0 m), and to assess the relative importance of environmental drivers. Then, independent validation was conducted using newly collected SOC measurements from 53 sites, together with systematic benchmarking against four prominent global or regional SOC datasets: SoilGrids (Poggio et al. 2021), HWSD (FAO and CAS 2023), WISE (Batjes 2016), and recent regional predictions by Mishra et al. (2021). Additionally, we evaluated spatial uncertainties by identifying regions where existing SOC estimates diverge most significantly among the mapping products. The specific objectives of this study were to: (1) Produce spatially explicit, high-resolution SOC stock estimates at distinct soil depth layers (0–0.3, 0.3–1.0, 1.0–2.0 m, and the total 0–2.0 m profile) across the entire QTP; (2) identify and quantify the relative importance of contemporary and historical environmental drivers influencing vertical and spatial distributions of SOC; and (3) generate validated SOC maps and delineate critical uncertainty hotspots to improve regional carbon accounting and inform sustainable land management strategies across the QTP under rapid environmental change. Collectively, this study provides a validated, high-resolution estimation of SOC stocks down to 2 across the whole QTP and offers critical insights for cold region carbon accounting and assessments of carbon–climate feedbacks under ongoing environmental change.

2 | Materials and Methods

2.1 | Study Region

The Qinghai-Tibet Plateau (QTP), often referred to as the "roof of the world," spans from 26°00′–39°47′ N to 73°19′–104°47′ E (Li et al. 2025), with an average elevation exceeding 4000 m (Bao et al. 2024). It is the largest and highest plateau on Earth, characterized by complex topography and pronounced spatial heterogeneity in climate, soils, and ecosystems. Vegetation exhibits a pronounced southeast-northwest gradient, ranging from

forests in humid, low-altitude regions to alpine meadows, shrublands, grasslands, and deserts in increasingly arid, high-altitude zones. Forests consist mainly of evergreen and deciduous species, while alpine vegetation dominates in colder, harsher environments (Fan and Bai 2021). Soils on the QTP are dominated by permafrost-affected Gelisols/cryosols and young mineral soils such as inceptisols, with notable areas of aridisols in the western plateau (Li et al. 2014). Human activities are generally limited but increasing in recent decades, such as grazing, land reclamation, and infrastructure development, which are modifying vegetation cover and soil processes in some regions (Wang et al. 2014; Peng et al. 2020; Zhu et al. 2023). These contrasting climatic conditions, landscape properties, and land cover/use types are expected to result in substantially variability in SOC storage, vertical distribution along the soil profile, and underlying controlling factors.

Especially, the QTP contains the most extensive permafrost area at middle and low latitudes, covering approximately $1.30 \times 10^6\,km^2$, or 42% of the plateau's surface, with an average active layer thickness of $2.34 \pm 0.70\,m$ (Wang et al. 2020). The permafrost would exert strong control over SOC stabilization, particularly the vertical transportation and distribution along the soil profile induced by cryoturbation. This cryoturbation and associated frequent freeze–thaw cycles would lead to distinct SOC turnover behaviors compared to other regions, resulting in that SOC dynamics on the QTP cannot be predicted using models developed in other regions less affected by permafrost.

2.2 | Data Collection

We assembled the most comprehensive dataset of SOC measurements currently available for the QTP, comprising 2442 soil profiles with SOC content (SOC_c, g C kg^{-1} soil) measured in the fine earth fraction (< 2 mm) (Table S1). Data were integrated from multiple sources, including public databases, national surveys, historical records, and peer-reviewed literature: (1) The World Soil Information Service (WoSIS, https://www.isric.org/explore/wosis): SOC data from the QTP region extracted from this global soil database; (2) Second National Soil Census: Soil profile data collected across the QTP during China's second national soil survey (Pan and Shi 2015); (3) Historical survey records: Regional soil surveys reported in government publications for Tibet and its administrative divisions; (4) Published peer-reviewed literature: SOC profiles from peer-reviewed studies conducted across the QTP (Yang et al. 2008; Mu et al. 2015; Ding et al. 2016; Zhao et al. 2018; Liu et al. 2019; Chen et al. 2021; Cheng et al. 2021; Gao, Zhang, et al. 2021). Although the soil profiles were compiled from different periods and methods, data scarcity across the QTP necessitated integrating all available sources. Given that spatial variability of SOC at the regional scale far exceeds temporal or methodological differences, the assembled dataset provides the most representative basis currently available for large-scale analysis.

To facilitate cross-profile comparisons, SOC_c was harmonized to four depth layers (0–0.3, 0.3–1.0, 1.0–2.0 m and the full profile 0–2.0 m) using mass-preserving splines (Bishop et al. 1999; Malone et al. 2009), which are widely used in digital soil mapping (Batjes et al. 2024; Wang, Filippi, et al. 2024). We used this approach by fitting a smooth depth function at 1 cm resolution to discrete SOC observations while preserving the total SOC mass across the original sampling depth intervals, thereby minimizing distortion during depth harmonization. For profiles with SOC stock (SOC_s, t C ha^{-1}) reported, we directly used the reported SOC_s. For profiles without SOC_s reported directly, SOC_s were calculated for each depth interval using:

$$soc_s = \frac{soc_c}{100} \times D \times BD \times \left(1 - \frac{G}{100}\right) \times 10$$

where D is the soil depth (i.e., 0.3, 0.7, 1.0, or 2.0 m in this study), BD is the bulk density of the fine earth fraction < 2 mm ($kg\,m^{-3}$), and G is the gravel content (> 2 mm, % by volume). Missing BD values were estimated using a generalized XGBoost model (Wang, Guo, et al. 2022; Wang, Zhang, et al. 2025) to ensure the full dataset was retained for subsequent analyses.

2.3 | Environmental Covariates

Seven categories of environmental factors—climate, paleoclimate, topography, vegetation dynamics, human activities, lithology, and permafrost type—were selected, comprising 71 environmental covariates (Table S2). These factors represent major biophysical controls on SOC formation, stabilization, and redistribution in the region. Climatic variables regulate SOC accumulation and turnover by controlling plant productivity and microbial decomposition (Schlesinger and Andrews 2000; Davidson and Janssens 2006), whereas paleoclimatic variables capture legacy effects of historical climate conditions on soil development and SOC preservation, particularly in permafrost regions (Ding et al. 2019). Topographic attributes influence microclimate, hydrological pathways, and erosion–deposition processes, thereby shaping spatial patterns of soil moisture and SOC redistribution, which would be particularly important on the QTP (Li et al. 2022; Hu et al. 2025; Xu et al. 2025). Vegetation-related variables (e.g., vegetation type and NDVI) serve as proxies for organic matter inputs and ecosystem productivity (Stockmann et al. 2015). Human activity indicators reflect land-use disturbances that modify vegetation cover and soil properties, affecting SOC dynamics (Wang et al. 2014; Peng et al. 2020; Ren et al. 2025). Lithology and permafrost type further constrain SOC dynamics by controlling soil mineralogy, thermal regimes, and freeze–thaw processes that govern SOC stabilization (Batjes 2016; Chen et al. 2024). Together, these covariates benchmarks modeling of the spatial and vertical variability of SOC across the QTP.

Specifically, 11 temperature variables and eight precipitation variables were obtained from the WorldClim v2.0 (https://www.worldclim.org/data), with a spatial resolution of 30 arcseconds, equal to about 1 km (Hijmans et al. 2005; Fick and Hijmans 2017). Because the variation of climatic variables within each 1 km grid cell is generally minimal, the subsequent resampling to 90 m resolution introduced only negligible errors. In brief, these climate variables were calculated based on climate station records during the period 1970–2000, representing a long-term average. Additionally, paleoclimate data, including 19 climate variables of the Mid-Holocene (about 6000 years ago) and the Last Glacial

Maximum (about 22,000 years ago), were also obtained from the WorldClim v2.0.

Seven topographic attributes were considered in this study, including elevation, slope, aspect, curvature, topographic wetness index, slope length and steepness factor and topographic roughness index. The elevation data are derived from the Shuttle Radar Topography Mission 4.0 (SRTM4.0). The remaining six variables were extracted and calculated from ArcGIS, SAGA-GIS (http://www.saga-gis.org), RSAGA and other geographic software or R packages.

Vegetation properties include normalized differential vegetation index (NDVI) and vegetation type. The NDVI data were from the MODIS product MOD13Q1006 (https://ladsweb.modaps.eosdis.nasa.gov/). Average values from the period 2001 to 2018 were used in this study. Averaging across this time span provides a more robust representation of the long-term vegetation condition, thereby reducing the influence of interannual variability. The vegetation type was derived from the vegetation map of China (https://www.plantplus.cn/doi/10.12282/plantdata.0155) (Zhang 2007).

Human activities include human land use, livestock density, and human population. The land use data were derived from land use maps interpreted from Landsat Thematic Mapper (TM) satellite imagery, provided by the Resource and Environment Science and Data Center, the Chinese Academy of Sciences (http://www.resdc.cn). Population data (https://landscan.ornl.gov/landscan-datasets) were derived from the LandScan Global Vital Statistics Analysis database. The data on livestock density (http://data.tpdc.ac.cn) were derived from the National QTP Scientific Data Center, representing the actual animal density at the county level in 2010. Human activities would be the most time-relevant variables with limited data to quantify their temporal variability, changes over time, which could introduce uncertainty into our SOC estimates by altering carbon inputs, vegetation cover, and soil properties at different temporal scales.

Lithology type (https://www.geo.uni-hamburg.de/en/geologie/forschung/aquatische-geochemie/glim.html) was used to reflect 15 types of soil rocks and parent materials, and derived from the Global Lithological Map Database v1.0. Three permafrost types, including permafrost, seasonally frozen permafrost, and nonfrozen soil (https://data.tpdc.ac.cn/), were derived from the National QTP Scientific Data Center.

2.4 | Driver Analysis and Digital Mapping

A machine learning model, random forest (RF), was trained to explain the variability of SOC_s across the region using the 71 environmental predictors (Table S2). In addition, we also included the starting and ending depth of the depth interval as two predictors, which allowed us to obtain one single three-dimensional model. RF was used because of its demonstrated ability to capture complex nonlinear relationships and interactions among environmental variables, as well as its strong performance when handling large, heterogeneous datasets (Breiman 2001). These characteristics make RF particularly suitable for regional-scale SOC mapping in environmentally complex regions such as the Qinghai–Tibet Plateau. Prior to model fitting, multicollinearity among environmental predictors was controlled using variance inflation factors (VIF) with the vif function in the car package in R (v4.1.1). Predictors with VIF values greater than 10 were excluded to reduce redundancy among highly correlated variables. However, several ecologically important predictors (e.g., mean annual temperature and mean annual precipitation) were preferentially retained, to ensure explicit representation of key climatic controls on SOC. We further evaluated the impact of this VIF-based screening strategy on model performance and found that cross-validated predictive accuracy was not substantially reduced after removing highly collinear variables. Model hyperparameters (mtry, randomly selected predictors; splitrule, splitting rule; min.node.size, minimal node size) were optimized by using a fivefold cross-validated approach using the train function in the caret package in R 4.1.1, with 80% of data used to train the RF model, and the remaining 20% data used to validate the model projections (Figure S1). The best RF model was selected with the highest coefficient of determination (R^2), followed by normalization of predictor importance, which was expressed as relative importance within the model.

To disentangle potential interrelationships among environmental drivers of SOC_s of different soil layers, we fitted structural equation models (SEM). The 71 candidate environmental variables were categorized into seven groups, representing latent constructs: climate, paleoclimate, topography, vegetation, human activities, lithology, and permafrost type. Similar to the random forest model, only variables passing collinearity screening (i.e., VIF < 10) were retained for the SEM. A partial least square approach (PLS) was implemented to fit SEM using the *plspm* package in R (version 4.3.2), which is well-suited for handling complex systems characterized by complex latent constructs and potential multicollinearity among observed indicators (Mao et al. 2022; Wang, Zhang, et al. 2025). All input variables were standardized (z-score transformation) to ensure comparability and to facilitate the interpretation of standardized path coefficients. To assess the stability and significance of path coefficients, nonparametric bootstrapping was performed with 200 resamples. The 95% bootstrap confidence interval was used to judge that whether the estimated path coefficients are significant.

The best three-dimensional model was used to map SOC_s in the 0–0.3, 0.3–1, 1–2, and 0–2 m depth layers at the spatial resolution of 90 m across the whole QTP. Before applying the model, we obtained depth to bedrock (DTB) data from the Global Depth to Bedrock Dataset for Earth System Modeling (http://globalchange.bnu.edu.cn/research/dtb.jsp) (Yan et al. 2020). For each grid cell, if DTB is less than 2.0 m, SOC_s were only predicted to the DTB. Predictors that are not at the resolution of 90 m (Table S2) were resampled to the target resolution. Specifically, all covariates were harmonized to a common 90 m grid. Continuous variables were resampled using bilinear interpolation, whereas categorical variables were resampled using nearest-neighbor assignment. Although resampling from coarser-resolution datasets may introduce uncertainty at fine spatial scales, the resampled covariates mainly represent broad-scale environmental gradients (e.g., climate) that exhibit limited variability at local scales. Given the regional scope of this study, the potential influence of resampling on SOC prediction accuracy is expected to be limited.

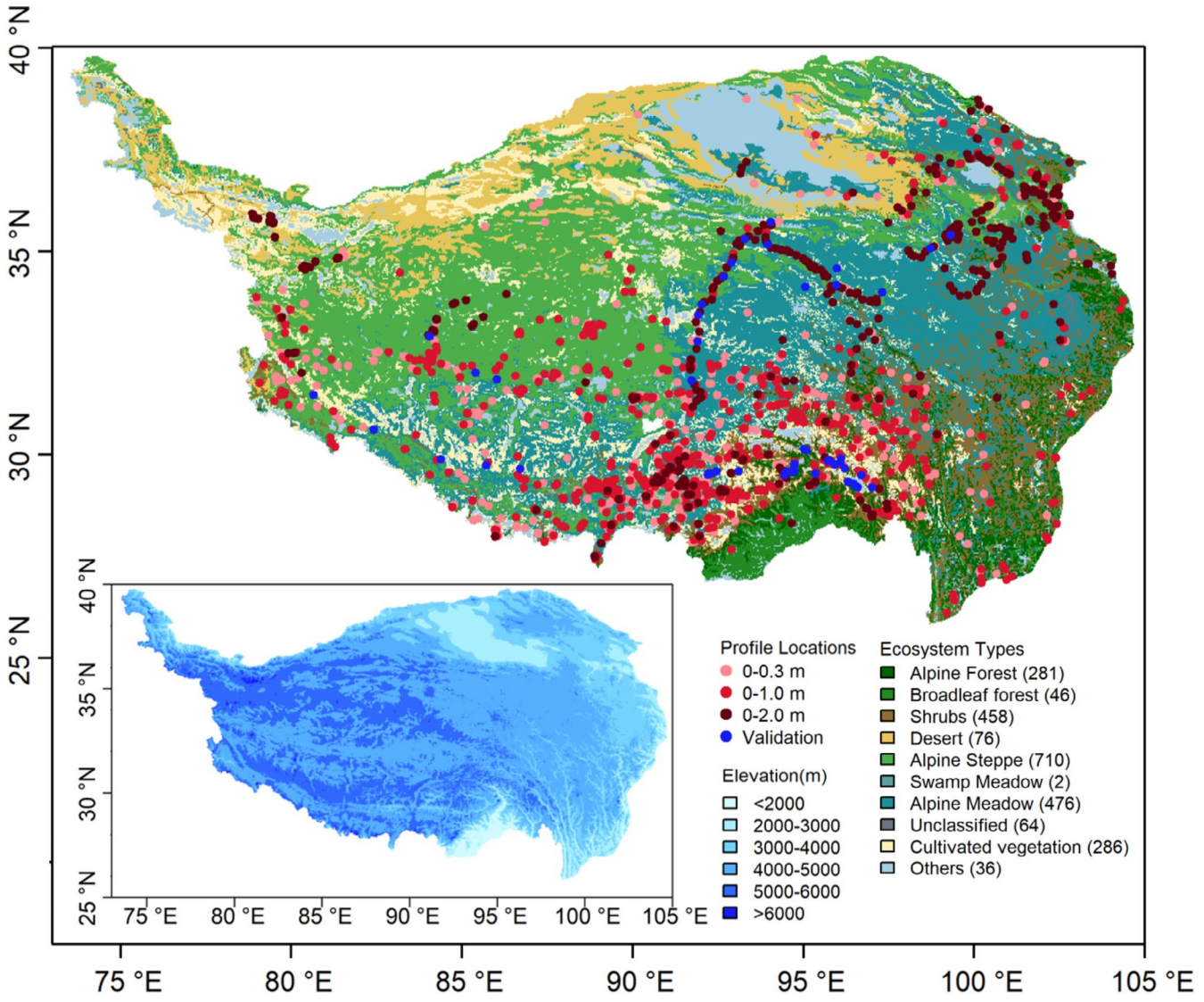

FIGURE 1 | Location of soil carbon profile on the Qinghai-Tibet Plateau. Red dots represent profiles compiled from multiple published and publicly available sources and used for model development, with sampled soil depth distinguished by different color densities. Blue dots indicate independent validation sites sampled by this study. The background map shows vegetation types classified into 10 categories with the corresponding profile numbers showed in the parentheses. The inset shows the elevation map of the study area, highlighting the altitudinal gradients across the plateau.

For each grid cell, the predicted SOC_s was represented by the mean of the 500 estimates produced by the individual trees of the fitted RF model, and the uncertainty was expressed as the 95% confidence interval of these estimates.

2.5 | Field Sampling

To derive an independent dataset to test our model, we additionally selected 53 points on the QTP with different elevations and climatic conditions to sample soils for SOC measurements (Figure 1). The elevation of the sampling points ranges from 1648 to 5373 m with a mean annual temperature (MAT) ranging from −5.90°C to 13.93°C and mean annual precipitation (MAP) ranging from 66 to 1316 mm. The test sites encompass major vegetation types on the QTP, including alpine forest, broadleaf forest, shrubland, alpine steppe, alpine meadow, and cultivated vegetation. These ecosystem types together occupy the vast majority of the plateau's land area and represent the dominant ecological gradients controlling SOC variability across the region. Measured SOCs values (the 53 validation sites) were compared with predicted SOC values at the corresponding locations, and the coefficient of determination (R^2) was calculated.

Soils at the 53 sites were sampled and analyzed using standardized field protocols and laboratory methods, ensuring comparability and high data quality (Mao et al. 2022). In brief, soil samples were collected from two depth intervals (0–0.3 and 0.3–1.0 m; sampling to depth of > 1.0 m in this study was constrained by logistical challenges in high-altitude and permafrost-affected environments). After transporting to the laboratory, the soil samples were air-dried at room temperature and then sieved to 2 mm to remove stones and visible roots. The air-dried samples were used to determine SOC content and bulk density, each measured in triplicate, and the average values were used to calculate SOC stocks.

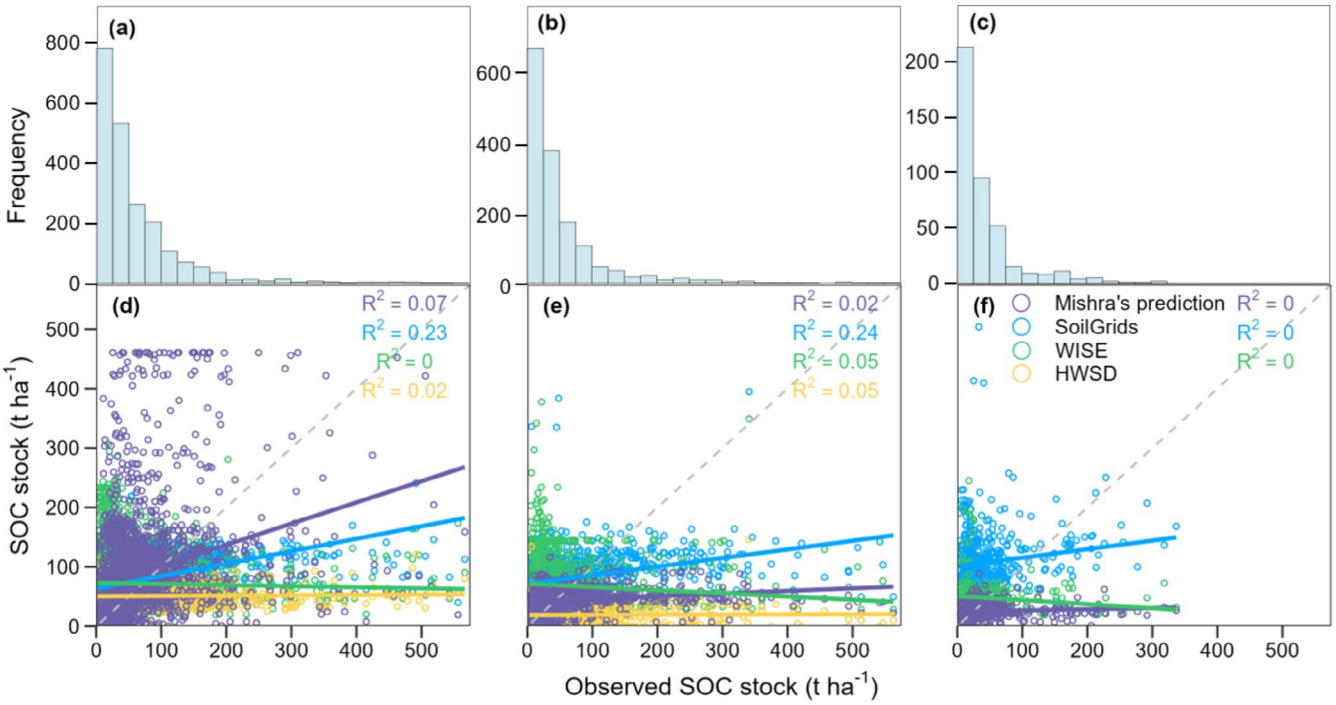

FIGURE 2 | Distributions of observed SOC stocks (SOC_s) and comparisons with global mapping products. (a–c) The frequency distribution of the observed SOC_s values, illustrating the range and skewness of SOC_s at 0–0.3 m (a), 0.3–1.0 m (b), and 1.0–2.0 m (c). (d–f) Comparison between observed and predicted SOC_s values from four mapping products at 0–0.3 m (d), 0.3–1.0 m (e), and 1.0–2.0 m (f), with R^2 values indicating the determination coefficient.

2.6 | Comparison With Other Mapping Products

To demonstrate the credibility of our estimates and identify regions with relatively high uncertainties, we compared our estimates with those in the same QTP region included in three global mapping products of SOC: SoilGrids (Poggio et al. 2021), WISE (Batjes 2016), and HWSD (FAO and CAS 2023). These datasets are among the most established global SOC estimates and are frequently used in large-scale carbon modeling and environmental assessments. This comparison was conducted for four standardized depth intervals (0–0.3, 0.3–1.0, 1.0–2.0, and 0–2.0 m), with a harmonization of the original datasets. For SoilGrids, SOC values in the four specific depth intervals were aggregated from reported layers. WISE and HWSD, which do not report SOC_s for the required depth intervals, estimated SOC stocks based on SOC content, bulk density, and gravel content provided by mapping products and interpolated to match using mass-preserving splines (Bishop et al. 1999; Malone et al. 2009).

For each grid cell, we estimated the percentage relative difference by calculating the difference between our estimates and those from the other products divided by our estimates. To assess the spatial variability among the four SOC_s estimates, we calculated the coefficient of variation (CV) at each grid cell across our mapping product and SoilGrids, WISE, HWSD. In pixels where one or more datasets lacked estimates (due to some discrepancies in spatial coverage of different products), the CV was computed using the available data. These comparisons enabled a comprehensive evaluation of the spatial pattern of uncertainties in current mapping products, highlighting regions with significant divergence among predictions. To ensure consistency across datasets with different resolutions and minimize discrepancies, we aggregated our 90 m resolution mapping products to a resolution of 1 km.

At last, using SOC data from the 53 sampled sites, we evaluated the accuracy of our mapping product, SoilGrids, WISE, HWSD, and a regional product focusing on the permafrost region (Mishra et al. 2021).

3 | Results

3.1 | Observed SOC Stocks Across the QTP

Our compiled dataset of 2442 soil profiles shows that surface SOC_s (0–0.3 m) across the QTP range from 1.4 to 1055.5 $t\,ha^{-1}$ (equivalent to a SOC content of 0.6–361.3 $g\,kg^{-1}$), with an average of 67.6 $t\,ha^{-1}$ (24.7 $g\,kg^{-1}$) and a median of 43.9 $t\,ha^{-1}$ (15.0 $g\,kg^{-1}$, Figure 2a). At greater depths, SOC_s range from 2.9 to 2475.2 $t\,ha^{-1}$ (0.4–344.9 $g\,kg^{-1}$) in the 0.3–1 m layer and 1.6 to 4080.9 $t\,ha^{-1}$ (0.03–403.5 $g\,kg^{-1}$) in the 1.0–2.0-m layer, with corresponding average values of 52.8 $t\,ha^{-1}$ (10.7 $g\,kg^{-1}$, Figure 2b) and 57.4 $t\,ha^{-1}$ (7.1 $g\,kg^{-1}$, Figure 2c). Notably, nearly two-thirds of the total SOC stored in the top 2 m resides below 0.3 m, highlighting the importance of subsoil carbon in this high-altitude region.

SOC_s differ significantly among vegetation types across all depth intervals ($p < 0.001$; Table 1). In the top 0–0.3 m layer, swamp meadow ecosystems exhibit the highest SOC_s (mean: 526.8 $t\,ha^{-1}$), followed by broadleaf forests (100.9 $t\,ha^{-1}$), alpine forests (98.8 $t\,ha^{-1}$), and alpine meadows (92.0 $t\,ha^{-1}$). Lower SOC_s are observed in shrublands (64.9 $t\,ha^{-1}$), cultivated

TABLE 1 | Observed soil organic carbon stocks (SOC_s) in different layers (0–0.3, 0.3–1.0, 1.0–2.0, 0–2.0 m) among ecosystem types on the QTP.

	SOC_s ($t\,ha^{-1}$)			
Ecosystem types	**0–0.3 m**	**0.3–1.0 m**	**1.0–2.0 m**	**0–2.0 m**
Swamp meadow	526.8	1035.3	—	—
Broadleaf forest	100.9 (83.0–118.8)	104.6 (75.6–133.6)	110.6 (50.5–170.8)	228.1 (180.3–275.8)
Alpine meadow	92.0 (82.4–101.6)	78.4 (61.5–95.4)	90.6 (32.7–148.4)	196.9 (162.1–231.6)
Alpine forest	98.8 (90.1–107.5)	65.5 (55.5–75.5)	56.3 (26.2–86.4)	169.6 (151.9–187.2)
Others	62.8 (36.5–89.2)	56.2 (17.6–94.8)	110.7 (−26.4–247.8)	131.3 (62.7–200.0)
Shrubs	64.9 (59.1–70.7)	42.9 (38.1–47.7)	38.9 (31.0–46.7)	111.8 (102.3–121.3)
Cultivated vegetation	53.3 (47.6–59.1)	48.6 (42.3–54.9)	42.6 (33.9–51.4)	108.1 (97.1–119.0)
Alpine steppe	44.1 (39.5–48.6)	36.9 (33.2–40.6)	41.5 (36.0–47.0)	92.0 (83.8–100.2)
Unclassified	46.6 (30.5–62.7)	26.6 (14.8–38.5)	21.0 (7.9–34.2)	75.4 (49.4–101.3)
Desert	18.7 (14.3–23.1)	21.4 (16.2–26.6)	33.9 (22.9–44.9)	53.7 (40.8–66.6)

Note: Values in parentheses are the 95% confidence intervals of SOC_s. No CIs for swamp meadow soils due to small sample size ($n = 2$); no SOC_s reported for swamp meadows at 1.0–2.0 and 0–2.0 m due to lack of profiles.

lands (53.3 $t\,ha^{-1}$), unclassified (46.6 $t\,ha^{-1}$), and alpine steppes (44.1 $t\,ha^{-1}$), with deserts having the lowest SOC_s (18.7 $t\,ha^{-1}$).

In the 0.3–1.0 m layer, swamp meadows again show the highest SOC_s (mean: 1035.3 $t\,ha^{-1}$), underscoring their strong carbon sequestration capacity at depth. Broadleaf forests (104.6 $t\,ha^{-1}$), alpine meadows (78.4 $t\,ha^{-1}$), and alpine forest (65.5 $t\,ha^{-1}$) retain relatively high SOC_s, while shrublands (42.9 $t\,ha^{-1}$), alpine steppe (36.9 $t\,ha^{-1}$), and deserts (21.4 $t\,ha^{-1}$) show lower values. SOC_s decline across all vegetation types in the 1.0–2.0 m layer, though broadleaf forests (110.6 $t\,ha^{-1}$) and alpine meadows (90.6 $t\,ha^{-1}$) continue to store substantial carbon. Swamp meadow data are sparse in this layer, likely due to sampling challenges in waterlogged soils.

3.2 | Controls on SOC_s Distribution

The random forest (RF) model integrating climate, paleoclimate, topography, vegetation, human activity, lithology, permafrost type, and soil depth explained 51% of the variance in SOC_s across soil layers (Figure 3).

Among individual predictors, normalized difference vegetation index (NDVI) was most influential, accounting for 10.2% of the variance. SOC_s showed a strong positive relationship with NDVI, reflecting vegetation productivity as a key driver of carbon input and thus SOC stocks. Mean annual precipitation ranked second in importance, followed by precipitation seasonality, paleo-precipitation seasonality from the Last Glacial Maximum, and mean annual temperature. Specifically, mean annual precipitation, mean annual precipitation, and mean diurnal range of temperature contributed 9.1%, 5.6%, and 5.1% to the explained variance of SOC, respectively. Topographic variables including topographic roughness index (4.6%) and topographic wetness index (4.2%) also played an important role. Paleoclimate variables, including precipitation seasonality of the Last Glacial Maximum and mean diurnal range

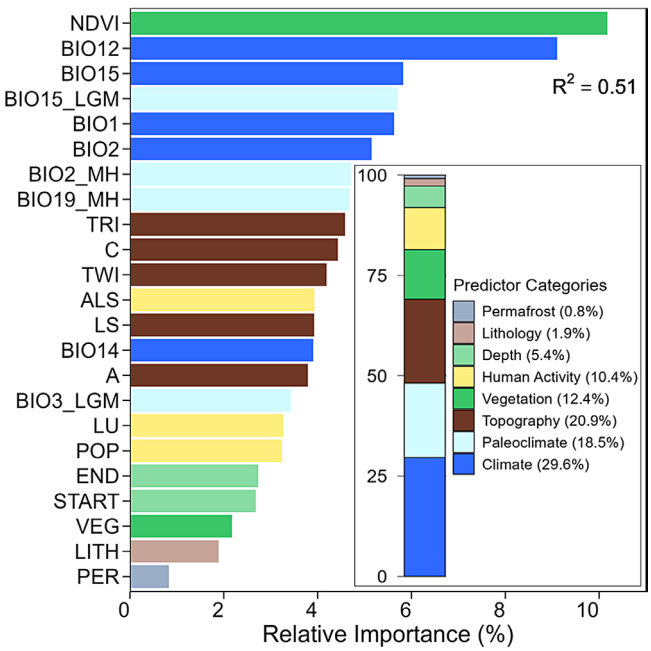

FIGURE 3 | Relative importance of environmental factors for predicting soil organic carbon stocks (SOC_s). A, aspect; ALS, carrying capacity; BIO1, annual mean temperature; Bio12, annual precipitation; BIO14, precipitation of driest month; BIO15, precipitation seasonality; BIO15_LGM, precipitation seasonality of the Last Glacial Maximum; BIO19_MH, precipitation of coldest quarter of the Mid-Holocene; BIO2, mean diurnal range; BIO2_MH, mean diurnal range of the Mid-Holocene; BIO3_LGM, isothermality of Last Glacial Maximum; C, curvature; END, ending depth of the soil layer; LITH, lithology; LS, slope length and steepness factor; LU, land use type; NDVI, normalized difference vegetation index; PER, permafrost type; POP, population; START, starting depth of the soil layer; TRI, Topographic roughness index; TWI, topographic wetness index; VEG, vegetation type. R^2 show the determination coefficients of the verification set. The bottom right inset summarizes the summed relative importance of eight environmental categories distinguished color.

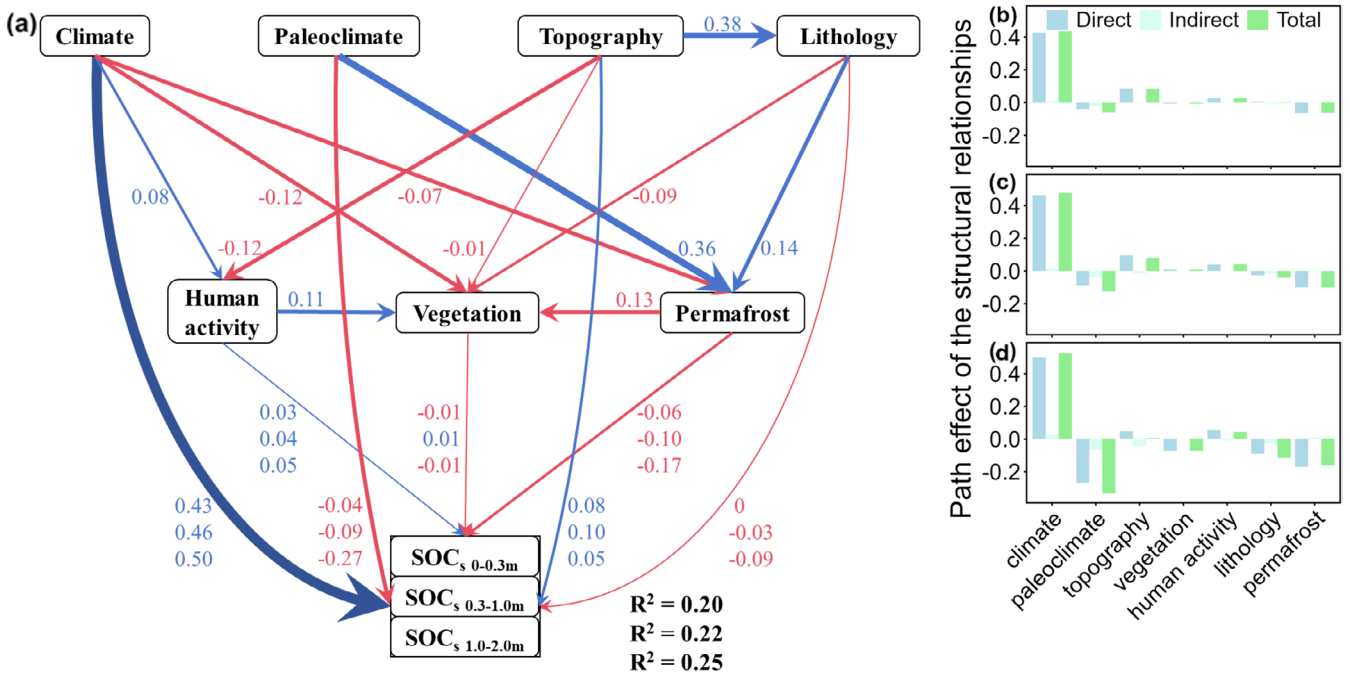

FIGURE 4 | Path analysis results of the controls over SOC stocks in three depth intervals. (a) Direct and indirect effects of seven latent variables on the SOC_s of different layers. The numbers show the path coefficients, with one set of values in three rows representing the coefficients for the three soil depth layers from top to bottom, and with a single value representing indirect effects which is independent of soil depth. The arrows indicate the effect direction, while the red and blue paths indicate that the effect is significantly ($p < 0.05$) negative and positive, respectively. The magnitude of the path coefficients is also represented by the arrow width. The indicators for the relevant latent variables are shown in Table S2. R^2 shows the determination coefficient for the corresponding variable, indicating the variance explained by the model. (b–d) Standardized direct, indirect, and total effects of the seven latent variables in the path analyses. The total effect is defined as the sum of direct and indirect effects.

of the Mid-Holocene, explained 5.7% and 4.7%, respectively, reflecting past climate influences on current SOC storage. Human activity factors, like livestock carrying capacity, land use type, and population, accounted for 3.9%, 3.3%, and 3.2%, respectively, revealing the importance of human activities for influencing SOC on the QTP.

When aggregated into predictor groups, contemporary climate explained the largest share of explained variance (29.6%), followed by topography (20.9%), paleoclimate (18.5%), vegetation (12.4%), and human activity (10.4%; Figure 3). Path analysis further revealed that contemporary climate exerted the strongest direct effects on SOC_s at all depths ($\rho = 0.43$–0.50), while topography was influential in topsoil ($\rho = 0.08$) and subsoil ($\rho = 0.10$). Paleoclimate had strong indirect effects via permafrost extent but negatively influenced SOC_s in deeper layers ($\rho = -0.27$; Figure 4). These interactions highlight the combined influence of current and legacy climatic conditions on soil carbon storage across the QTP.

3.3 | Spatial Patterns of SOC Stocks

We compared our observed SOC data with four global mapping products (SoilGrids, WISE, HWSD, Mishra et al. 2021). All four consistently overestimated SOC_s at low observed values and underestimated at high values, resulting in low predictive accuracy ($R^2 < 0.3$ across all depths; Figure 2). In contrast, our RF model, trained on the compiled dataset, achieved a cross-validated R^2 of 0.51, outperforming existing products. When validated against a separate set of 53 new sampling sites, the model achieved R^2 values of 0.63 and 0.49 for the 0–0.3 m and 0.3–1.0 m layers, respectively (Figure 5).

Using our model, we mapped SOC_s across the QTP at 90 m resolution (Figure 6a,d,g,j). SOC_s shows a clear southeast-to-northwest decline across all layers. Mean SOC_s was estimated at 207.7 (95% confidence interval: 184.0–231.4) t C ha^{-1} (0–2.0 m), 72.9 (65.0–80.8) t C ha^{-1} (0–0.3 m), 70.7 (62.1–79.4) t C ha^{-1} (0.3–1.0 m), and 64.1 (55.0–73.0) t C ha^{-1} (1.0–2.0 m). Total SOC stock in the 0–2 m profile across the QTP was estimated at 62.0 (54.9–69.1) Pg C, with 35%, 34%, and 31% stored in the 0–0.3 m, 0.3–1.0 m, and 1.0–2.0 m layers, respectively.

Among ecosystems, alpine meadows stored the largest total SOC (22.88 Pg C), followed by shrublands (10.33 Pg C), alpine steppes (9.57 Pg C), alpine forests (6.17 Pg C), and unclassified ecosystems (4.81 Pg C). Broadleaf forests (2.42 Pg C), deserts (2.05 Pg C), cultivated land (0.58 Pg C), and swamp meadows (0.36 Pg C) contributed less to the total SOC stocks (Figure 6c,f,i,l), primarily due to their limited spatial extent across the QTP. Compared to existing datasets, our total 0–2 m SOC estimate is lower than that from SoilGrids but higher than estimates from WISE and HWSD (Figure S3).

3.4 | Uncertainty and Variability

Despite improvements compared to existing mapping products, considerable uncertainty remains, particularly in the western QTP where data are sparse (Figure 6b,e,h,k). We calculated the

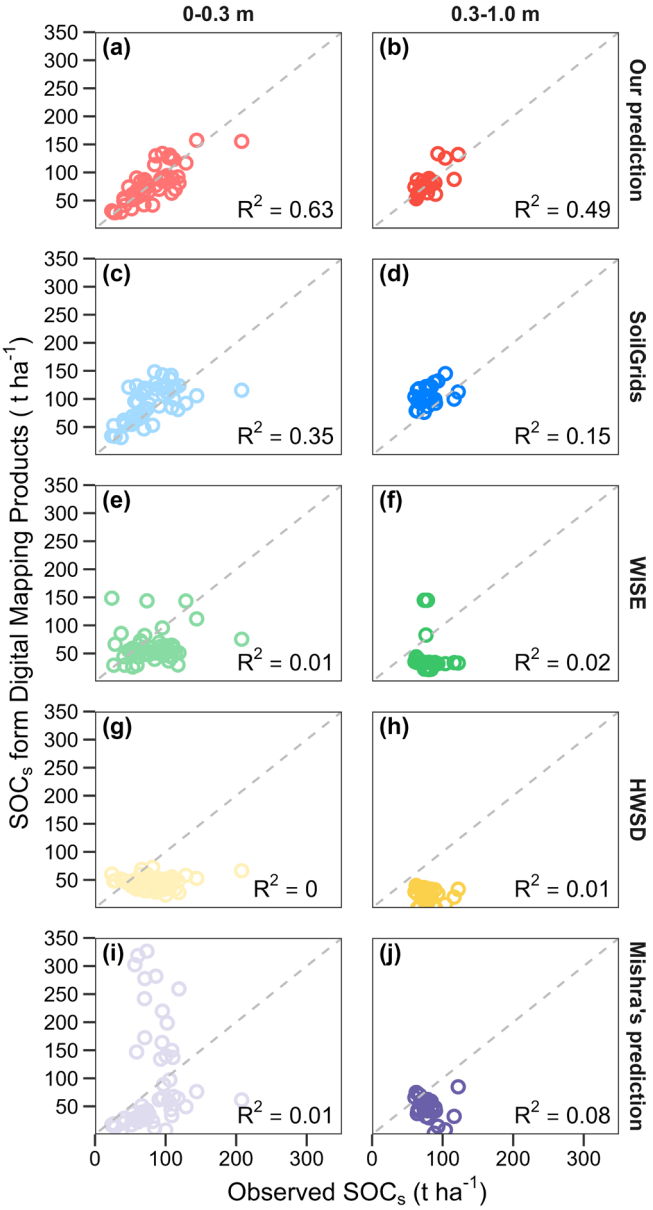

FIGURE 5 | Independent verification of five mapping products. From top to bottom, comparison of the measurements at 53 verification sites with our mapping products, SoilGrids, WISE, HWSD, Mishra's prediction, respectively. Left and right panels show the results for the 0–0.3 m and 0.3–1.0 m depths, respectively.

coefficient of variation (CV) across four SOC mapping products to assess inter-product variability (Figure 7). Mean CVs were 46.0% (0–0.3 m), 48.5% (0.3–1.0 m), 57.5% (1.0–2.0 m), and 46.1% (0–2.0 m). The highest uncertainties were observed in central and northeastern QTP, especially in the Qaidam Basin and alpine desert regions. CVs also varied by ecosystem. Desert, grassland, and "other" vegetation types showed the highest uncertainty across depths (e.g., CV > 60%), while alpine meadows, cropland, and unclassified had lower variability (CV < 50%). Notably, alpine meadows showed the lowest uncertainty in the deepest layers, reinforcing their value for regional carbon accounting.

4 | Discussion

Building upon a comprehensive dataset, this study provides a high-resolution mapping of SOC stocks down to 2 m depth across the QTP, thereby improving regional carbon accounting in one of the world's most climate-sensitive ecosystems. Our findings reveal that a substantial proportion (30.8%) of the total SOC stock is stored in the subsoils (typically 1.0–2.0 m), which is consistent with global studies indicating that a substantial proportion of SOC is stored below 30 cm (Jackson et al. 2017). This important component of the SOC stock remains underrepresented in many global and regional inventories. Although deep SOC is often assumed to be relatively stable, its vulnerability under ongoing environmental changes—including permafrost thaw and altered hydrological regimes—remains poorly constrained (Gao, Wang, et al. 2021; Zhang et al. 2022). These results underscore the critical need to incorporate deep-soil carbon dynamics of permafrost ecosystems into Earth system models, which currently focus largely on surface layers and may underestimate long-term carbon-climate feedbacks.

We observed pronounced spatial heterogeneity in SOC_s across the QTP, shaped by the region's biophysical complexity and by interactions among climate, vegetation, and topography. Among individual predictors, NDVI, precipitation, and precipitation seasonality emerged as key predictors. Across environmental covariate categories, climate emerged as the dominant driver, however, the RF model attributed a higher relative importance to vegetation than the SEM model. This discrepancy may reflect nonlinear climate effects on vegetation that are not fully captured by the SEM framework. NDVI, in particular, integrates both biomass production and microenvironmental conditions (e.g., moisture and temperature), offering a proxy for both SOC inputs and decomposition (Zehetgruber et al. 2017; San Román et al. 2024). Under environmental change, altered precipitation patterns and vegetation shifts may either exacerbate or buffer SOC losses (Zhang et al. 2015; Ding et al. 2019; Zhao et al. 2021; Yan et al. 2022; Ren et al. 2025). Thus, vegetation should be viewed as both a driver and a mediator of climate impacts on SOC, and its role should be explicitly incorporated into SOC prediction frameworks.

Our refined estimate of SOC stocks of 62.0 Pg C in the upper 2 m depth of QTP soils confirms the region as a globally significant high-altitude carbon reservoir (Chen, Ju, et al. 2022). However, this estimate diverges from global estimates such as SoilGrids (79.0 Pg C), WISE (46.9 Pg C), HWSD (30.0 Pg C), highlighting substantial uncertainties in current global spatial estimates. These discrepancies may reflect differences in model structures, training datasets, and predictor sensitivity, particularly in regions with complex topography and sparse observations. For example, we found that in alpine meadow and alpine steppe, SoilGrids and HWSD predicted higher SOC, likely due to their coarser resolution and broader generalizations, while our model better captured the SOC variability in these ecosystems (Figure 7). Compared to SoilGrids and HWSD, WISE performed relatively better in these areas, providing predictions closer to ours. In contrast, in desert and swamp meadow, WISE generally predicted lower SOC compared to SoilGrids, HWSD and

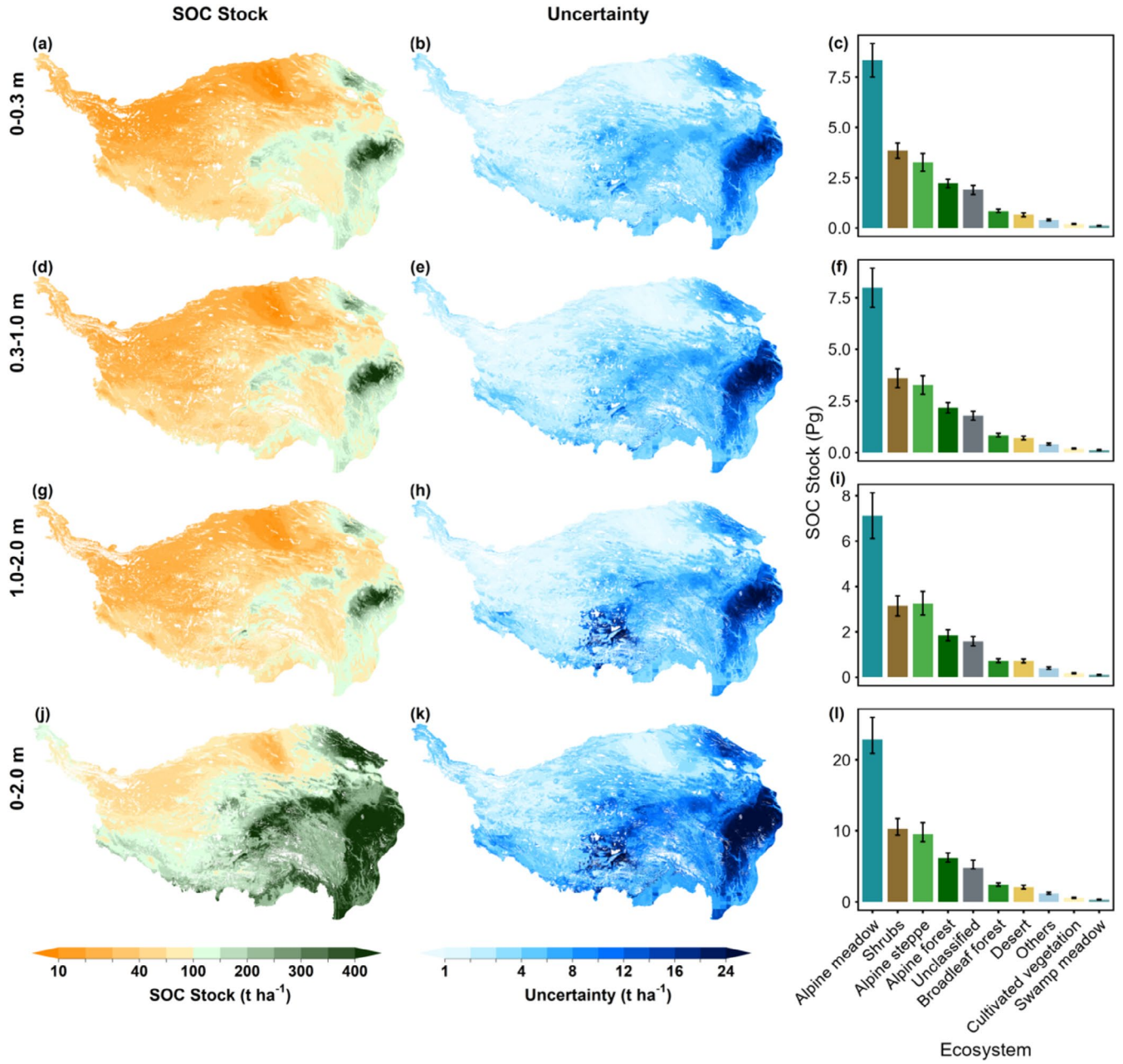

FIGURE 6 | Spatial distribution of soil organic carbon stocks and their uncertainties. Panels from top to bottom: Four soil layer depths (i.e., 0–0.3, 0.3–1.0, 1.0–2.0, 0–2.0 m), respectively. Panels from left to right: Soil organic carbon stocks; stock uncertainties represented by the standard error (SE) of ensemble predictions; and stock distribution among vegetation types with error bars indicating the 95% confidence intervals.

the estimates in this study. In regions with unclassified or other vegetation types, all three databases predicted lower SOC than ours. These differences underscore the importance of regionally calibrated approaches to better reflect regional ecological properties. Notably, several regional-scale estimates focusing on the same 0–2 m depth interval on the QTP have estimated a SOC stock of 37.71 Pg (Wang et al. 2021) and 40.11 Pg (Han et al. 2022), which are also lower than our estimates. These differences may largely stem from the heterogeneities in spatial coverage of the data used for model development.

We identified pronounced spatial uncertainty in SOC estimates, with hotspots concentrated in the Qaidam Basin and adjacent alpine steppe-desert transition zones. These areas exhibited the highest coefficients of variation (CVs) among datasets, which may be induced by sparse observations, complex terrain attributes, and novel climate-plant–soil interactions. This pattern is consistent with previous studies highlighting the challenges of SOC_s quantification in ecologically fragile, data-poor dryland regions (Wang, Kumar, et al. 2024). The arid climate and patchy vegetation in these zones amplify spatial heterogeneity in carbon stocks, inhibiting representative soil sampling and development of accurate models (Stanley et al. 2023; Ou et al. 2024; Wang, Sun, et al. 2025). In contrast, the southeastern QTP, dominated by alpine meadows and cultivated vegetation with higher observational density, exhibited lower uncertainty, underscoring the critical role of observational density and ecosystem homogeneities in reducing estimation errors (Ding et al. 2016, 2017; Han

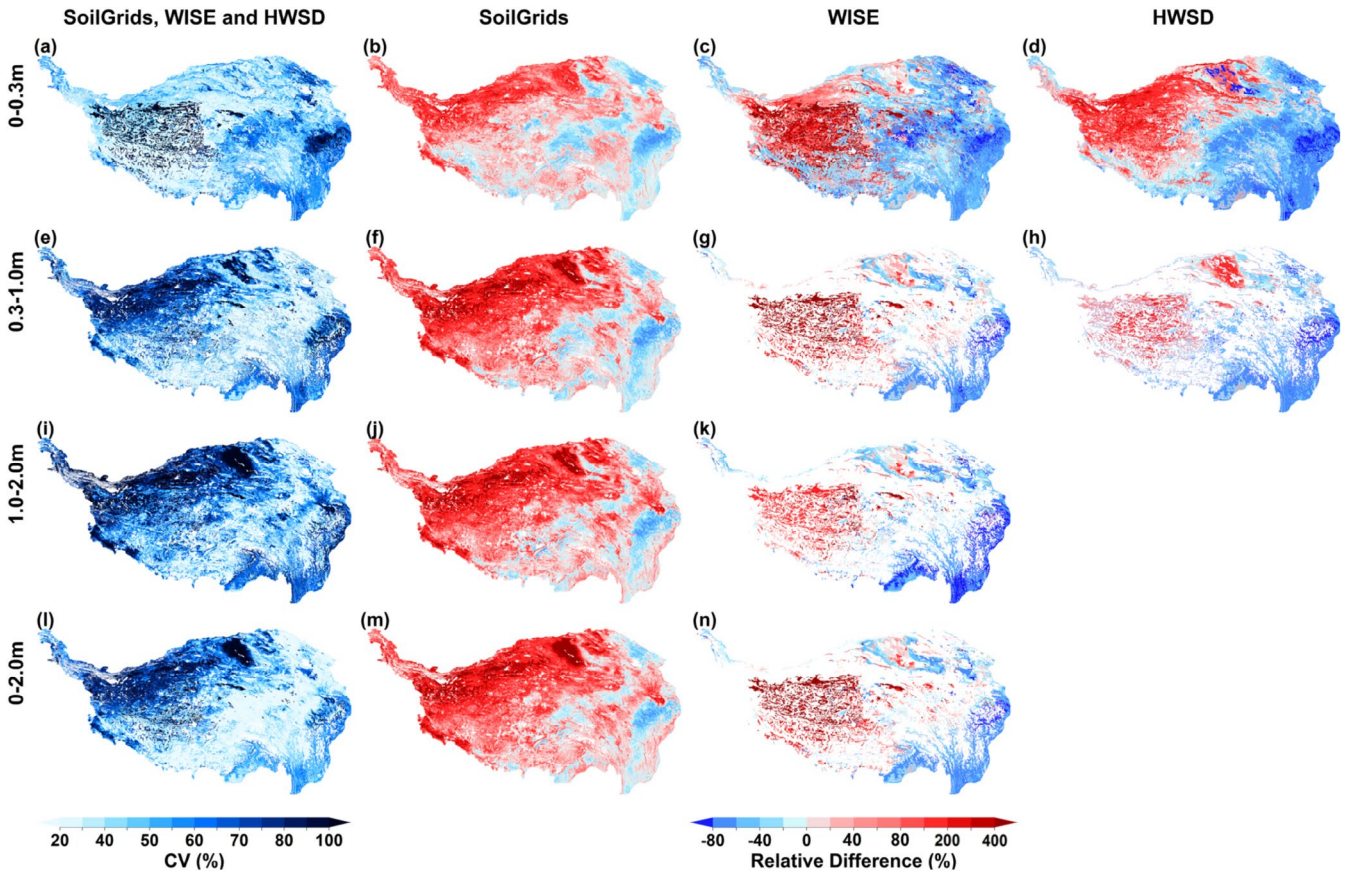

FIGURE 7 | Comparison of our estimates of soil organic carbon stocks with that in three global databases. Panels from left to right: The coefficient of variation (CV) of our predictions, SoilGrids, WISE, HWSD; the percentage relative difference between our prediction and SoilGrids, WISE, and HWSD, respectively. Panels from top to bottom show the results for the four soil depth layers (0–0.3, 0.3–1.0, 1.0–2.0, and 0–2.0 m). HSWD only estimated the 0–1 m soil depth.

et al. 2022). These spatial patterns provide strategic guidance for future monitoring studies, indicating that future sampling and model refinement efforts should prioritize uncertainty hotspots to improve reliability of SOC inventories.

Despite providing the depth-resolved and spatial-explicit SOC estimates to date for the QTP, our study has several limitations. First, while our analysis quantified SOC stocks to a depth of 2 m, many areas—particularly under alpine grasslands and alpine meadows—have soils extending well beyond this depth. Depth-to-bedrock data indicate that 90.8% of our study area exceeds 2 m in depth, and 87.4% exceeds 3 m, suggesting our total SOC stock estimate is likely conservative. Future efforts should aim to extend measurements and models to greater depths, particularly in regions with deeper soils. Second, although the 90 m spatial resolution captures broad-scale variation, many surface processes on the QTP—especially in mountainous areas like the Himalayas—occur at finer spatial scales. Microclimatic heterogeneity, topographic variation, and abrupt biome transitions occur over meters rather than tens of meters. Accurately representing SOC patterns in such environments will require integrating high-resolution environmental data and expanding the spatial granularity of SOC models. Third, our study does not explicitly account for permafrost dynamics. The QTP contains widespread permafrost, where SOC stabilization is strongly mediated by the seasonal dynamics of the active layer and the depth of the talik. Due to limited sample coverage in permafrost zones—particularly below the active layer—our stratified soil layers (0–0.3, 0.3–1.0, and 1.0–2.0 m) may not correspond to actual freeze–thaw boundaries. This mismatch could lead to under- or overestimation of SOC vulnerability in frozen soils, calling for better integration of thermal and hydrological data in future assessments.

5 | Conclusions

This study presents the most comprehensive and spatially explicit quantification of soil organic carbon (SOC) across the Qinghai-Tibetan Plateau (QTP) to date, providing both a valuable data resource and advancing conceptual understanding of depth-dependent SOC dynamics. Our results reveal pronounced vertical stratification and spatial heterogeneity in SOC distribution, shaped jointly by contemporary climatic conditions and paleoclimatic legacies, including historical permafrost extent. Surface-layer SOC (0–0.3 m) is largely governed by present-day vegetation characteristics and precipitation patterns, while deeper-layer SOC (1.0–2.0 m) predominantly reflects the influence of historical climatic regimes. These depth-dependent controls highlight the importance of integrating both contemporary and paleoenvironmental variables (e.g., vegetation type, precipitation regime, historical permafrost conditions)

into SOC modeling frameworks, particularly within alpine and permafrost-dominated ecosystems. Benchmarking our high-resolution SOC map against three global soil databases (e.g., SoilGrids, HWSD, WISE) revealed substantial discrepancies in low-data regions, further emphasizing the need for region-specific, observation-informed models. The datasets and insights generated in this study have direct implications for Earth system modeling (refining carbon–climate feedback projections), carbon budgeting (enhancing regional carbon inventory accuracy), and land management (guiding sustainable practices and conservation efforts). To address remaining knowledge gaps in QTP carbon dynamics, future efforts should: (1) extend sampling beyond 2 m depth in key ecosystems; (2) intensify observational efforts in uncertainty hotspots such as the Qaidam Basin and ecotonal zones; and (3) develop high-resolution models integrating remote sensing and localized field observations. In permafrost regions, coordinated efforts are particularly essential to quantify SOC distributions across freeze–thaw layers and evaluate their responses to climate-induced thaw.

Author Contributions

Feng Liu: writing – review and editing. **Mishra Umakant:** writing – review and editing. **Yuanhe Yang:** writing – review and editing. **Zhou Shi:** writing – review and editing. **Zhongkui Luo:** conceptualization, writing – review and editing, investigation, funding acquisition, supervision, data curation. **Shuai Zhang:** investigation, writing – review and editing. **Jiajun Mao:** data curation, investigation, writing – original draft, writing – review and editing, visualization. **Mingming Wang:** data curation, review and editing. **Wu Yu:** data curation.

Acknowledgments

Contributions of U. Mishra were supported through a U.S. Department of Energy grant to the Sandia National Laboratories, which is a multi-mission laboratory managed and operated by National Technology and Engineering Solutions of Sandia LLC, a wholly owned subsidiary of Honeywell International Inc., for the U.S. Department of Energy's National Nuclear Security Administration under contract DE-NA-0003525.

Funding

This research was financially supported by the National Natural Science Foundation of China (grant no. 32241036) and Zhejiang Provincial Natural Science Foundation of China (grant no. LZ25D030001).

Conflicts of Interest

The authors declare no conflicts of interest.

Data Availability Statement

The data and code that support the findings of this study are openly available at Figshare at https://doi.org/10.6084/m9.figshare.31429055. The soil profile data were obtained from World Soil Information Service at https://www.isric.org/explore/wosis. The environmental covariates include climate data obtained from WorldClim v2.0 at https://www.worldclim.org/data. Paleoclimate data were also sourced from WorldClim v2.0. Topographic data were derived from Shuttle Radar Topography Mission 4.0 (SRTM4.0). Vegetation data, including Normalized Difference Vegetation Index (NDVI) data, were obtained from the MODIS product MOD13Q1006 at https://ladsweb.modaps.eosdis.nasa.gov/, while vegetation type data were sourced from the vegetation map of China at https://www.plantplus.cn/doi/10.12282/plantdata.0155. Human activity data, including human land use data from Landsat Thematic Mapper (TM) satellite imagery at http://www.resdc.cn, population data from the LandScan Global Vital Statistics Analysis database at https://landscan.ornl.gov/landscan-datasets, and livestock density data from the National QTP Scientific Data Center at http://data.tpdc.ac.cn. Lithology data were obtained from the Global Lithological Map Database v1.0 at https://www.geo.uni-hamburg.de/en/geologie/forschung/aquatische-geochemie/glim.html. Permafrost data were sourced from the National QTP Scientific Data Center at https://data.tpdc.ac.cn/.

References

Bao, F. L., H. Letu, H. Z. Shang, et al. 2024. "Advancing Cloud Classification Over the Tibetan Plateau: A New Algorithm Reveals Seasonal and Diurnal Variations." *Geophysical Research Letters* 51: e2024GL109590.

Batjes, N. H. 2016. "Harmonized Soil Property Values for Broad-Scale Modelling (WISE30sec) With Estimates of Global Soil Carbon Stocks." *Geoderma* 269: 61–68.

Batjes, N. H., L. Calisto, and L. M. de Sousa. 2024. "Providing Quality-Assessed and Standardised Soil Data to Support Global Mapping and Modelling (WoSIS Snapshot 2023)." *Earth System Science Data* 16: 4735–4765.

Bishop, T. F. A., A. B. McBratney, and G. M. Laslett. 1999. "Modelling Soil Attribute Depth Functions With Equal-Area Quadratic Smoothing Splines." *Geoderma* 91: 27–45.

Bolch, T., A. Kulkarni, A. Kääb, et al. 2012. "The State and Fate of Himalayan Glaciers." *Science* 336: 310–314.

Breiman, L. 2001. "Random Forests." *Machine Learning* 45: 5–32.

Cao, Y.-Z., X.-D. Wang, X.-Y. Lu, Y. Yan, and J.-H. Fan. 2013. "Soil Organic Carbon and Nutrients Along an Alpine Grassland Transect Across Northern Tibet." *Journal of Mountain Science* 10: 564–573.

Chang, X. F., S. P. Wang, S. J. Cui, et al. 2014. "Alpine Grassland Soil Organic Carbon Stock and Its Uncertainty in the Three Rivers Source Region of the Tibetan Plateau." *PLoS One* 9, no. 5: e97140.

Chen, H., P. J. Ju, Q. Zhu, et al. 2022. "Carbon and Nitrogen Cycling on the Qinghai-Tibetan Plateau." *Nature Reviews Earth & Environment* 3: 701–716.

Chen, J., J. Zhang, T. H. Wu, et al. 2022. "Activity and Kinematics of Two Adjacent Freeze-Thaw-Related Landslides Revealed by Multisource Remote Sensing of Qilian Mountain." *Remote Sensing* 14: 5059.

Chen, L. Y., G. B. Yang, Y. X. Bai, et al. 2024. "Permafrost Carbon Cycle and Its Dynamics on the Tibetan Plateau." *Science China. Life Sciences* 67: 1833–1848.

Chen, Q., Y. Yuan, Y. Hu, et al. 2021. "Excessive Nitrogen Addition Accelerates N Assimilation and P Utilization by Enhancing Organic Carbon Decomposition in a Tibetan Alpine Steppe." *Science of the Total Environment* 764: 142848.

Cheng, H., B. Wu, M. Wei, et al. 2021. "Changes in Community Structure and Metabolic Function of Soil Bacteria Depending on the Type Restoration Processing in the Degraded Alpine Grassland Ecosystems in Northern Tibet." *Science of the Total Environment* 755: 142619.

Crowther, T. W., K. E. O. Todd-Brown, C. W. Rowe, et al. 2016. "Quantifying Global Soil Carbon Losses in Response to Warming." *Nature* 540: 104–108.

Davidson, E. A., and I. A. Janssens. 2006. "Temperature Sensitivity of Soil Carbon Decomposition and Feedbacks to Climate Change." *Nature* 440: 165–173.

Ding, J., L. Chen, C. Ji, et al. 2017. "Decadal Soil Carbon Accumulation Across Tibetan Permafrost Regions." *Nature Geoscience* 10: 420–424.

Ding, J., F. Li, G. Yang, et al. 2016. "The Permafrost Carbon Inventory on the Tibetan Plateau: A New Evaluation Using Deep Sediment Cores." *Global Change Biology* 22: 2688–2701.

Ding, J., T. Wang, S. Piao, et al. 2019. "The Paleoclimatic Footprint in the Soil Carbon Stock of the Tibetan Permafrost Region." *Nature Communications* 10: 4195.

Fan, Z. M., and X. Y. Bai. 2021. "Scenarios of Potential Vegetation Distribution in the Different Gradient Zones of Qinghai-Tibet Plateau Under Future Climate Change." *Science of the Total Environment* 796: 148918.

FAO, I., ISRIC, ESBN, and CAS. 2023. "Harmonized World Soil Database v2.0 (v2.01)."

Fick, S. E., and R. J. Hijmans. 2017. "WorldClim 2: New 1-Km Spatial Resolution Climate Surfaces for Global Land Areas." *International Journal of Climatology* 37: 4302–4315.

Fu, Z. T., Q. B. Wu, A. P. Chen, et al. 2025. "Non-Temperature Environmental Drivers Modulate Warming-Induced 21st-Century Permafrost Degradation on the Tibetan Plateau (vol 16, 7556, 2025)." *Nature Communications* 16: 10036.

Gao, H. K., J. J. Wang, Y. Z. Yang, X. C. Pan, Y. J. Ding, and Z. Duan. 2021. "Permafrost Hydrology of the Qinghai-Tibet Plateau: A Review of Processes and Modeling." *Frontiers in Earth Science* 8: 576838.

Gao, T., Y. Zhang, S. Kang, et al. 2021. "Accelerating Permafrost Collapse on the Eastern Tibetan Plateau." *Environmental Research Letters* 16: 54023.

Garcia-Palacios, P., M. A. Bradford, I. Benavente-Ferraces, et al. 2024. "Dominance of Particulate Organic Carbon in Top Mineral Soils in Cold Regions." *Nature Geoscience* 17: 145–150.

Han, D., Z. Hu, X. Wang, et al. 2022. "Shift in Controlling Factors of Carbon Stocks Across Biomes on the Qinghai-Tibetan Plateau." *Environmental Research Letters* 17: 74016.

Hijmans, R. J., S. E. Cameron, J. L. Parra, P. G. Jones, and A. Jarvis. 2005. "Very High Resolution Interpolated Climate Surfaces for Global Land Areas." *International Journal of Climatology* 25: 1965–1978.

Hu, Z. G., J. C. Svenning, J. W. Tang, et al. 2025. "Distributions and Drivers of Soil Organic Carbon on the Tibetan Plateau: Divergent Controls Across Ecosystems." *Plant and Soil* 516: 1993–2012.

Huang, J. P., X. J. Zhou, G. X. Wu, et al. 2023. "Global Climate Impacts of Land-Surface and Atmospheric Processes Over the Tibetan Plateau." *Reviews of Geophysics* 61: e2022RG000771.

Hugelius, G., J. Strauss, S. Zubrzycki, et al. 2014. "Estimated Stocks of Circumpolar Permafrost Carbon With Quantified Uncertainty Ranges and Identified Data Gaps." *Biogeosciences* 11: 6573–6593.

Jackson, R. B., K. Lajtha, S. E. Crow, G. Hugelius, M. G. Kramer, and G. Piñeiro. 2017. "The Ecology of Soil Carbon: Pools, Vulnerabilities, and Biotic and Abiotic Controls." *Annual Review of Ecology, Evolution, and Systematics* 48: 419–445.

Jenny, H. 1941. *Factors of Soil Formation: A System of Quantitative Pedology*. Dover Publications.

Jiang, L., H. Chen, Q. Zhu, et al. 2019. "Assessment of Frozen Ground Organic Carbon Pool on the Qinghai-Tibet Plateau." *Journal of Soils and Sediments* 19: 128–139.

Kuttippurath, J., V. K. Patel, and B. R. Sharma. 2024. "Observed Changes in the Climate and Snow Dynamics of the Third Pole." *npj Climate and Atmospheric Science* 7: 162.

Li, H. Y., F. G. Liu, S. P. Zhang, et al. 2022. "Drying-Wetting Changes of Surface Soil Moisture and the Influencing Factors in Permafrost Regions of the Qinghai-Tibet Plateau, China." *Remote Sensing* 14: 2915.

Li, W. P., L. Zhao, X. D. Wu, et al. 2014. "Distribution of Soils and Landform Relationships in Permafrost Regions of the Western Qinghai-Xizang (Tibetan) Plateau, China." *Soil Science* 179: 348–357.

Li, Y. Z., C. J. Li, W. X. Zhou, et al. 2025. "Identification of Conservation Priority Areas on the Qinghai-Tibet Plateau Considering Habitat, Biodiversity, Ecosystem Services, and Human Well-Being." *Journal of Environmental Management* 393: 127113.

Liang, Z., S. Chen, Y. Yang, R. Zhao, Z. Shi, and R. A. Viscarra Rossel. 2019. "National Digital Soil Map of Organic Matter in Topsoil and Its Associated Uncertainty in 1980's China." *Geoderma* 335: 47–56.

Liu, L., H. Chen, L. Jiang, et al. 2019. "Response of Anaerobic Mineralization of Different Depths Peat Carbon to Warming on Zoige Plateau." *Geoderma* 337: 1218–1226.

Malone, B. P., A. B. McBratney, B. Minasny, and G. M. Laslett. 2009. "Mapping Continuous Depth Functions of Soil Carbon Storage and Available Water Capacity." *Geoderma* 154: 138–152.

Mao, X. L., J. Y. Zheng, W. Yu, et al. 2022. "Climate-Induced Shifts in Composition and Protection Regulate Temperature Sensitivity of Carbon Decomposition Through Soil Profile." *Soil Biology & Biochemistry* 172: 108743.

Mishra, U., G. Hugelius, E. Shelef, and Y. H. Yang. 2021. "Spatial Heterogeneity and Environmental Predictors of Permafrost Region Soil Organic Carbon Stocks." *Science Advances* 7: eaaz5236.

Mu, C., B. W. Abbott, A. J. Norris, et al. 2020. "The Status and Stability of Permafrost Carbon on the Tibetan Plateau." *Earth-Science Reviews* 211: 103433.

Mu, C., T. Zhang, Q. Wu, et al. 2015. "Editorial: Organic Carbon Pools in Permafrost Regions on the Qinghai–Xizang (Tibetan) Plateau." *Cryosphere* 9: 479–486.

Ou, J. X., Z. H. Wu, Q. W. Yan, X. Y. Feng, and Z. L. Zhao. 2024. "Improving Soil Organic Carbon Mapping in Farmlands Using Machine Learning Models and Complex Cropping System Information." *Environmental Sciences Europe* 36: 80.

Pan, X., and J. Shi. 2015. *Profile Database of Typical Soils From the Second National Soil Survey of China (1980–1996)*. National Earth System Science Data Center.

Peng, F., X. Xue, Q. You, et al. 2020. "Change in the Trade-Off Between Aboveground and Belowground Biomass of Alpine Grassland: Implications for the Land Degradation Process." *Land Degradation & Development* 31: 105–117.

Poggio, L., L. M. de Sousa, N. H. Batjes, et al. 2021. "SoilGrids 2.0: Producing Soil Information for the Globe With Quantified Spatial Uncertainty." *Soil* 7: 217–240.

Ren, S., T. Wang, X. H. Ji, et al. 2025. "Grazing Reverses Climate-Induced Soil Carbon Gains on the Tibetan Plateau." *Nature Communications* 16: 6978.

San Román, A. X., N. Srikanthan, A. A. Hamid, et al. 2024. "Long-Term Warming in a Temperate Forest Accelerates Soil Organic Matter Decomposition Despite Increased Plant-Derived Inputs." *Biogeochemistry* 167: 1159–1174.

Schlesinger, W. H., and J. A. Andrews. 2000. "Soil Respiration and the Global Carbon Cycle." *Biogeochemistry* 48: 7–20.

Schuur, E. A. G., A. D. McGuire, C. Schädel, et al. 2015. "Climate Change and the Permafrost Carbon Feedback." *Nature* 520: 171–179.

Slomp, C. P., C. Dörfer, P. Kühn, F. Baumann, J.-S. He, and T. Scholten. 2013. "Soil Organic Carbon Pools and Stocks in Permafrost-Affected Soils on the Tibetan Plateau." *PLoS One* 8: e57024.

Stanley, P., J. Spertus, J. Chiartas, P. B. Stark, and T. Bowles. 2023. "Valid Inferences About Soil Carbon in Heterogeneous Landscapes." *Geoderma* 430: 116323.

Stockmann, U., J. Padarian, A. McBratney, et al. 2015. "Global Soil Organic Carbon Assessment." *Global Food Security* 6: 9–16.

Tarnocai, C., J. G. Canadell, E. A. G. Schuur, P. Kuhry, G. Mazhitova, and S. Zimov. 2009. "Soil Organic Carbon Pools in the Northern Circumpolar Permafrost Region." *Global Biogeochemical Cycles* 23: GB2023.

von Lützow, M., and I. Kögel-Knabner. 2009. "Temperature Sensitivity of Soil Organic Matter Decomposition-What Do We Know?" *Biology and Fertility of Soils* 46: 1–15.

Wang, D. 2022. "Digital Soil Mapping in Tibetan Plateau Permafrost Regions." *Nature Reviews Earth & Environment* 3: 3.

Wang, D., T. Wu, L. Zhao, et al. 2021. "A 1 Km Resolution Soil Organic Carbon Dataset for Frozen Ground in the Third Pole." *Earth System Science Data* 13: 3453–3465.

Wang, J., P. Filippi, S. Haan, L. Pozza, B. Whelan, and T. F. Bishop. 2024. "Gaussian Process Regression for Three-Dimensional Soil Mapping Over Multiple Spatial Supports." *Geoderma* 446: 116899.

Wang, M. M., X. W. Guo, S. Zhang, et al. 2022. "Global Soil Profiles Indicate Depth-Dependent Soil Carbon Losses Under a Warmer Climate." *Nature Communications* 13: 5514.

Wang, M. M., S. Zhang, X. W. Guo, et al. 2025. "Whole-Profile Soil Carbon Responses to Concurrent Warming and Precipitation Changes Across Global Biomes." *Global Change Biology* 31: e70105.

Wang, T., D. Yang, Y. Yang, et al. 2020. "Permafrost Thawing Puts the Frozen Carbon at Risk Over the Tibetan Plateau." *Science Advances* 6: eaaz3513.

Wang, X., S. Dong, B. Yang, Y. Li, and X. Su. 2014. "The Effects of Grassland Degradation on Plant Diversity, Primary Productivity, and Soil Fertility in the Alpine Region of Asia's Headwaters." *Environmental Monitoring and Assessment* 186: 6903–6917.

Wang, Y., Y. Sun, Q. Wang, et al. 2025. "Exploring the Spatial Heterogeneity of Soil Organic Carbon and the Influence of Coastal Factors: A Case Study in the Yellow River Delta, China." *Science of the Total Environment* 959: 178234.

Wang, Y. F., W. W. Lv, K. Xue, et al. 2022. "Grassland Changes and Adaptive Management on the Qinghai-Tibetan Plateau." *Nature Reviews Earth & Environment* 3: 668–683.

Wang, Z. N., J. Kumar, S. R. Weintraub-Leff, K. Todd-Brown, U. Mishra, and D. Sihi. 2024. "Upscaling Soil Organic Carbon Measurements at the Continental Scale Using Multivariate Clustering Analysis and Machine Learning." *Journal of Geophysical Research – Biogeosciences* 129: e2023JG007702.

Xu, J. P., M. X. Liu, S. Q. Mei, et al. 2025. "Characteristics and Controlling Factors of Soil Micro-Climate in a Subtropical Re-Vegetation Catchment: Insights From Continuous Moisture and Temperature Observations." *Plant and Soil* 519: 1–20.

Yan, F. P., S. G. Wei, J. Zhang, and B. F. Hu. 2020. "Depth-to-Bedrock Map of China at a Spatial Resolution of 100 Meters." *Scientific Data* 7: 2.

Yan, Y. J., S. L. Niu, Y. C. He, et al. 2022. "Changing Plant Species Composition and Richness Benefit Soil Carbon Sequestration Under Climate Warming." *Functional Ecology* 36: 2906–2916.

Yang, H. J., X. C. Shen, J. Yao, and Q. Wen. 2020. "Portraying the Impact of the Tibetan Plateau on Global Climate." *Journal of Climate* 33: 3565–3583.

Yang, M. X., X. J. Wang, G. J. Pang, G. N. Wang, and Z. C. Liu. 2019. "The Tibetan Plateau Cryosphere: Observations and Model Simulations for Current Status and Recent Changes." *Earth-Science Reviews* 190: 353–369.

Yang, Y., J. Fang, Y. Tang, et al. 2008. "Storage, Patterns and Controls of Soil Organic Carbon in the Tibetan Grasslands." *Global Change Biology* 14: 1592–1599.

Yang, Y. H., J. Y. Fang, P. Smith, et al. 2009. "Changes in Topsoil Carbon Stock in the Tibetan Grasslands Between the 1980s and 2004." *Global Change Biology* 15: 2723–2729.

Zehetgruber, B., J. Kobler, T. Dirnböck, R. Jandl, R. Seidl, and A. Schindlbacher. 2017. "Intensive Ground Vegetation Growth Mitigates the Carbon Loss After Forest Disturbance." *Plant and Soil* 420: 239–252.

Zhang, G. F., Z. T. Nan, N. Hu, et al. 2022. "Qinghai-Tibet Plateau Permafrost at Risk in the Late 21st Century." *Earth's Future* 10: e2022EF002652.

Zhang, K. R., H. S. Dang, Q. F. Zhang, and X. L. Cheng. 2015. "Soil Carbon Dynamics Following Land-Use Change Varied With Temperature and Precipitation Gradients: Evidence From Stable Isotopes." *Global Change Biology* 21: 2762–2772.

Zhang, S., M. M. Wang, L. J. Xiao, et al. 2024. "Reconciling Carbon Quality With Availability Predicts Temperature Sensitivity of Global Soil Carbon Mineralization." *Proceedings of the National Academy of Sciences of the United States of America* 121: e2313842121.

Zhang, X. S. 2007. *Vegetation Map of the People's Republic of China (1:1 000 000)*. Geology Press.

Zhao, F. B., Y. P. Wu, J. Y. Hui, B. Sivakumar, X. Y. Meng, and S. G. Liu. 2021. "Projected Soil Organic Carbon Loss in Response to Climate Warming and Soil Water Content in a Loess Watershed." *Carbon Balance and Management* 16: 24.

Zhao, L., X. Wu, Z. Wang, et al. 2018. "Soil Organic Carbon and Total Nitrogen Pools in Permafrost Zones of the Qinghai-Tibetan Plateau." *Scientific Reports* 8: 3656.

Zhu, L. K., A. R. Ives, C. Zhang, Y. Y. Guo, and V. C. Radeloff. 2019. "Climate Change Causes Functionally Colder Winters for Snow Cover-Dependent Organisms." *Nature Climate Change* 9: 886.

Zhu, Q., H. Chen, C. Peng, et al. 2023. "An Early Warning Signal for Grassland Degradation on the Qinghai-Tibetan Plateau." *Nature Communications* 14: 106641.

Zou, D. F., L. Zhao, Y. Sheng, et al. 2017. "A New Map of Permafrost Distribution on the Tibetan Plateau." *Cryosphere* 11: 2527–2542.

Supporting Information

Additional supporting information can be found online in the Supporting Information section. **Table S1:** Source of soil profiles with soil organic carbon measurements. **Table S2:** Information of environmental factors. **Table S3:** Comparison of mean values for numeric variables before and after resampling. **Figure S1:** Random forest model performance for driver analysis. The red line is the regression line of calibration set; the blue line is the regression line of validation set; the grey dashed line represents the 1:1 line. **Figure S2:** Random forest model performance of digital mapping. The red line is the regression line of calibration set; the blue line is the regression line of validation set; the grey dashed line represents the 1:1 line. **Figure S3:** Total soil organic carbon stocks on the QTP predicted by different mapping products. Error bars indicate the 95% confidence intervals of predictions.